The Astrophysical Journal, 675:1014–1024, 2008 March 10
© 2008. The American Astronomical Society. All rights reserved. Printed in U.S.A.

SEARCH FOR ULTRA–HIGH-ENERGY NEUTRINOS WITH AMANDA-II

M. Ackermann,[1] J. Adams,[2] J. Ahrens,[3] K. Andeen,[4] J. Auffenberg,[5] X. Bai,[6] B. Baret,[7] S. W. Barwick,[8] R. Bay,[9] K. Beattie,[10] T. Becka,[3] J. K. Becker,[11] K.-H. Becker,[5] M. Beimforde,[12] P. Berghaus,[13] D. Berley,[14] E. Bernardini,[1] D. Bertrand,[13] D. Z. Besson,[15] E. Blaufuss,[14] D. J. Boersma,[4] C. Bohm,[16] J. Bolmont,[1] S. Böser,[1] O. Botner,[17] A. Bouchta,[17] J. Braun,[4] T. Burgess,[16] T. Castermans,[18] D. Chirkin,[10] B. Christy,[14] J. Clem,[6] D. F. Cowen,[19,20] M. V. D'Agostino,[9] A. Davour,[17] C. T. Day,[10] C. De Clercq,[7] L. Demirörs,[6] F. Descamps,[21] P. Desiati,[4] G. de Vries-Uiterweerd,[22] T. DeYoung,[19] J. C. Diaz-Velez,[4] J. Dreyer,[11] J. P. Dumm,[4] M. R. Duvoort,[22] W. R. Edwards,[10] R. Ehrlich,[14] J. Eisch,[4] R. W. Ellsworth,[14] P. A. Evenson,[6] O. Fadiran,[23] A. R. Fazely,[24] K. Filimonov,[9] C. Finley,[4] M. M. Foerster,[19] B. D. Fox,[19] A. Franckowiak,[5] R. Franke,[1] T. K. Gaisser,[6] J. Gallagher,[25] R. Ganugapati,[4] H. Geenen,[5] L. Gerhardt,[8,26] A. Goldschmidt,[10] J. A. Goodman,[14] R. Gozzini,[3] T. Griesel,[3] A. Groß,[27] S. Grullon,[4] R. M. Gunasingha,[24] M. Gurtner,[5] C. Ha,[19] A. Hallgren,[17] F. Halzen,[4] K. Han,[2] K. Hanson,[4] D. Hardtke,[9] R. Hardtke,[28] Y. Hasegawa,[29] T. Hauschildt,[6] J. Heise,[22] K. Helbing,[5] M. Hellwig,[3] P. Herquet,[18] G. C. Hill,[4] J. Hodges,[4] K. D. Hoffman,[14] B. Hommez,[21] K. Hoshina,[4] D. Hubert,[7] B. Hughey,[4] J.-P. Hülß,[30] P. O. Hulth,[16] K. Hultqvist,[16] S. Hundertmark,[16] M. Inaba,[29] A. Ishihara,[29] J. Jacobsen,[4] G. S. Japaridze,[23] H. Johansson,[16] J. M. Joseph,[10] K.-H. Kampert,[5] A. Kappes,[4,31] T. Karg,[5] A. Karle,[4] H. Kawai,[29] J. L. Kelley,[4] J. Kiryluk,[10] F. Kislat,[12] N. Kitamura,[4] S. R. Klein,[10] S. Klepser,[1] G. Kohnen,[18] H. Kolanoski,[12] L. Köpke,[3] M. Kowalski,[12] T. Kowarik,[3] M. Krasberg,[4] K. Kuehn,[8] T. Kuwabara,[6] M. Labare,[13] K. Laihem,[30] H. Landsman,[4] R. Lauer,[1] H. Leich,[1] D. Leier,[11] I. Liubarsky,[32] J. Lundberg,[17] J. Lünemann,[11] J. Madsen,[28] R. Maruyama,[4] K. Mase,[29] H. S. Matis,[10] T. McCauley,[10] C. P. McParland,[10] K. Meagher,[14] A. Meli,[11] T. Messarius,[11] P. Mészáros,[19,20] H. Miyamoto,[29] T. Montaruli,[4,33] A. Morey,[9] R. Morse,[4] S. M. Movit,[20] K. Münich,[11] R. Nahnhauer,[1] J. W. Nam,[8] P. Nießen,[6] D. R. Nygren,[10] A. Olivas,[14] M. Ono,[29] S. Patton,[10] C. Pérez de los Heros,[17] A. Piegsa,[3] D. Pieloth,[1] A. C. Pohl,[17,34] R. Porrata,[9] J. Pretz,[14] P. B. Price,[9] G. T. Przybylski,[10] K. Rawlins,[35] S. Razzaque,[19,20] P. Redl,[14] E. Resconi,[27] W. Rhode,[11] M. Ribordy,[36] A. Rizzo,[7] S. Robbins,[5] W. J. Robbins,[19] P. Roth,[14] F. Rothmaier,[3] C. Rott,[19] C. Roucelle,[10] D. Rutledge,[19] D. Ryckbosch,[21] H.-G. Sander,[3] S. Sarkar,[37] K. Satalecka,[1] S. Schlenstedt,[1] T. Schmidt,[14] D. Schneider,[4] O. Schultz,[27] D. Seckel,[6] B. Semburg,[5] S. H. Seo,[19] Y. Sestayo,[27] S. Seunarine,[2] A. Silvestri,[8] A. J. Smith,[14] C. Song,[4] G. M. Spiczak,[28] C. Spiering,[1] M. Stamatikos,[4,38] T. Stanev,[6] T. Stezelberger,[10] R. G. Stokstad,[10] M. C. Stoufer,[10] S. Stoyanov,[6] E. A. Strahler,[4] T. Straszheim,[14] K.-H. Sulanke,[1] G. W. Sullivan,[14] T. J. Sumner,[32] Q. Swillens,[13] I. Taboada,[9] O. Tarasova,[1] A. Tepe,[5] L. Thollander,[16] S. Tilav,[6] M. Tluczykont,[1] P. A. Toale,[19] D. Tosi,[1] D. Turčan,[14] N. van Eijndhoven,[22] J. Vandenbroucke,[9] A. Van Overloop,[21] V. Viscomi,[19] C. Vogt,[30] B. Voigt,[1] W. Wagner,[19] C. Walck,[16] H. Waldmann,[1] T. Waldenmaier,[6] M. Walter,[1] Y.-R. Wang,[4] C. Wendt,[4] C. H. Wiebusch,[30] C. Wiedemann,[16] G. Wikström,[16] D. R. Williams,[19] R. Wischnewski,[1] H. Wissing,[30] K. Woschnagg,[9] X. W. Xu,[24] G. Yodh,[8] S. Yoshida,[29] and J. D. Zornoza[4,39]
(IceCube Collaboration)

Received 2007 September 14; accepted 2007 November 18

[1] DESY, D-15735 Zeuthen, Germany.
[2] Department of Physics and Astronomy, University of Canterbury, Private Bag 4800, Christchurch, New Zealand.
[3] Institute of Physics, University of Mainz, Staudinger Weg 7, D-55099 Mainz, Germany.
[4] Department of Physics, University of Wisconsin, Madison, WI 53706.
[5] Department of Physics, University of Wuppertal, D-42119 Wuppertal, Germany.
[6] Bartol Research Institute and Department of Physics and Astronomy, University of Delaware, Newark, DE 19716.
[7] Vrije Universiteit Brussel, Dienst ELEM, B-1050 Brussels, Belgium.
[8] Department of Physics and Astronomy, University of California, Irvine, CA 92697.
[9] Department of Physics, University of California, Berkeley, CA 94720.
[10] Lawrence Berkeley National Laboratory, Berkeley, CA 94720.
[11] Department of Physics, Universität Dortmund, D-44221 Dortmund, Germany.
[12] Institut für Physik, Humboldt-Universität zu Berlin, D-12489 Berlin, Germany.
[13] Université Libre de Bruxelles, Science Faculty CP230, B-1050 Brussels, Belgium.
[14] Department of Physics, University of Maryland, College Park, MD 20742.
[15] Department of Physics and Astronomy, University of Kansas, Lawrence, KS 66045.
[16] Department of Physics, Stockholm University, SE-10691 Stockholm, Sweden.
[17] Division of High Energy Physics, Uppsala University, S-75121 Uppsala, Sweden.
[18] University of Mons-Hainaut, 7000 Mons, Belgium.
[19] Department of Physics, Pennsylvania State University, University Park, PA 16802.
[20] Department of Astronomy and Astrophysics, Pennsylvania State University, University Park, PA 16802.
[21] Department of Subatomic and Radiation Physics, University of Gent, B-9000 Gent, Belgium.
[22] Department of Physics and Astronomy, Utrecht University/SRON, NL-3584 CC Utrecht, The Netherlands.
[23] CTSPS, Clark-Atlanta University, Atlanta, GA 30314.
[24] Department of Physics, Southern University, Baton Rouge, LA 70813.
[25] Department of Astronomy, University of Wisconsin, Madison, WI 53706.
[26] Corresponding author: gerhardt@hep.ps.uci.edu.
[27] Max-Planck-Institut für Kernphysik, D-69177 Heidelberg, Germany.
[28] Department of Physics, University of Wisconsin, River Falls, WI 54022.
[29] Department of Physics, Chiba University, Chiba 263-8522 Japan.
[30] III Physikalisches Institut, RWTH Aachen University, D-52056 Aachen, Germany.
[31] On leave of absence from Universität Erlangen-Nürnberg, Physikalisches Institut, D-91058, Erlangen, Germany.
[32] Blackett Laboratory, Imperial College, London SW7 2BW, UK.
[33] On leave of absence from Università di Bari, Dipartimento di Fisica, I-70126, Bari, Italy.
[34] Affiliated with School of Pure and Applied Natural Sciences, Kalmar University, S-39182 Kalmar, Sweden.

ABSTRACT

A search for diffuse neutrinos with energies in excess of 10^5 GeV is conducted with AMANDA-II data recorded between 2000 and 2002. Above 10^7 GeV, the Earth is essentially opaque to neutrinos. This fact, combined with the limited overburden of the AMANDA-II detector (roughly 1.5 km), concentrates these ultra–high-energy neutrinos at the horizon. The primary background for this analysis is bundles of downgoing, high-energy muons from the interaction of cosmic rays in the atmosphere. No statistically significant excess above the expected background is seen in the data, and an upper limit is set on the diffuse all-flavor neutrino flux of $E^2\Phi_{90\%\mathrm{CL}} < 2.7 \times 10^{-7}$ GeV cm^{-2} s^{-1} sr^{-1} valid over the energy range of 2×10^5 to 10^9 GeV. A number of models that predict neutrino fluxes from active galactic nuclei are excluded at the 90% confidence level.

Subject headings: diffuse radiation — galaxies: active — neutrinos — telescopes

1. INTRODUCTION

AMANDA-II (Antarctic Muon and Neutrino Detector Array), a neutrino telescope at the geographical South Pole designed to detect Cerenkov light from secondary particles produced in collisions between neutrinos and Antarctic ice, has placed limits on the flux from pointlike and diffuse sources of astrophysical neutrinos (Achterberg et al. 2007; Ackermann et al. 2004, 2005; Ahrens et al. 2003a, 2003b). This work describes a search for neutrinos with energies above 10^5 GeV, which we call ultra–high-energy (UHE) neutrinos. These neutrinos are of interest because they could be associated with the potential acceleration of hadrons by active galactic nuclei (Mannheim 1995; Mannheim et al. 2000; Halzen & Zas 1997; Protheroe 1997; Stecker et al. 1992); they could potentially be produced by exotic phenomena such as the decay of topological defects (Sigl et al. 1998) or possibly be associated with the *Z*-burst mechanism (Yoshida et al. 1998); and they are guaranteed by-products of the interactions of high-energy cosmic rays with the cosmic microwave background (Engel et al. 2001).

This analysis is sensitive to all three flavors of neutrinos. Leptons and cascades from UHE electron, muon, and tau neutrinos create bright, energetic events (Fig. 1) that can be identified by AMANDA-II as far as 450 m from the center of the array (Fig. 2). The sensitivity of this analysis starts at energies roughly coincident with the highest energy threshold of other diffuse analyses conducted with AMANDA-II (Achterberg et al. 2007; Ackermann et al. 2004).

At UHE energies, the interaction length of neutrinos in rock is shorter than the diameter of the Earth (Gandhi et al. 1998), so neutrinos from the Northern Hemisphere will interact before reaching AMANDA-II. Combined with the limited overburden above the AMANDA-II detector, this concentrates UHE events at the horizon. This contrasts with the majority of other astrophysical neutrino analyses completed using data from the AMANDA-II detector, which search for neutrinos from the Northern Hemisphere with energies below 10^5 GeV.

The flux of atmospheric neutrinos is negligible at UHE energies, with fewer than 10 events in 3 yr expected from the model in Lipari (1993) after intermediate UHE selection criteria have been applied. This drops to 0.1 events after application of all selection criteria. Similarly, there are fewer than 0.6 events expected in 3 yr at the final selection level from prompt neutrinos from the decay of charmed particles produced in the atmosphere (using the "C" model from Zas et al. 1993). Therefore, the primary background for the UHE analysis is composed of many lower energy processes that mimic higher energy signal events. Cosmic-ray collisions in the upper atmosphere that generate large numbers of nearly parallel muons (or "muon bundles") can generate high-energy signatures even though the individual muons have much lower energy than single leptons or cascades from UHE neutrinos. Signal and background events spread light over roughly equivalent areas in the detector, but UHE neutrino events are distinguishable because they have higher energy and higher light density than background events. Specialized selection criteria that use these properties, as well as differences in reconstruction variables, separate the UHE neutrinos from the background of muon bundles from atmospheric cosmic rays.

Limits have been placed on the all-flavor neutrino flux in the ultra–high-energy range by other experiments (Fig. 3). In addition, a previous analysis using an earlier configuration of the AMANDA detector called AMANDA-B10, consisting of 302 optical modules (Ackermann et al. 2005), has placed limits on the all-flavor UHE neutrino flux (Fig. 3). This analysis uses 677 optical modules (OMs) of the AMANDA-II detector and gives a combined result using data from three years (2000–2002) with a live time of 456.8 days.

A description of the AMANDA-II detector is given in § 2. Sections 3 and 4 discuss possible sources of astrophysical neutrinos and background, and the simulation of both. The selection criteria used to separate UHE neutrino signals from background are discussed in § 5. A study of systematic uncertainties is presented in § 6, and the results are shown in § 7.

2. THE AMANDA-II DETECTOR

The AMANDA-II detector (Ahrens et al. 2004a) consists of 677 OMs stationed between 1500 and 2000 m beneath the surface of the Antarctic ice at the geographic South Pole. The OMs are deployed on 19 vertical cables (called "strings") arranged in three roughly concentric circles, giving the detector a cylindrical shape with a diameter of approximately 200 m.

Each OM contains a Hamamatsu 8 inch (20.3 cm) photomultiplier tube (PMT) coupled with silicon gel to a spherical glass pressure housing for continuity of the index of refraction. The OMs are connected to the surface by cables that supply high voltage and carry the signal from the PMT to data acquisition electronics at the surface. The inner 10 strings use electrical analog signal transmission, while the outer nine strings primarily use optical fiber transmission (Ahrens et al. 2004a).

The AMANDA-II detector uses a majority trigger of 24 OMs recording a voltage above a set threshold (a "hit") within a time window of 2.5 μs. An OM records the maximum amplitude, as

[35] Department of Physics and Astronomy, University of Alaska Anchorage, 3211 Providence Dr., Anchorage, AK 99508.
[36] Laboratory for High Energy Physics, École Polytechnique Fédérale, CH-1015 Lausanne, Switzerland.
[37] Department of Physics, University of Oxford, 1 Keble Road, Oxford OX1 3NP, UK.
[38] NASA Goddard Space Flight Center, Greenbelt, MD 20771.
[39] Affiliated with IFIC (CSIC-Universitat de València), A. C. 22085, 46071 Valencia, Spain.

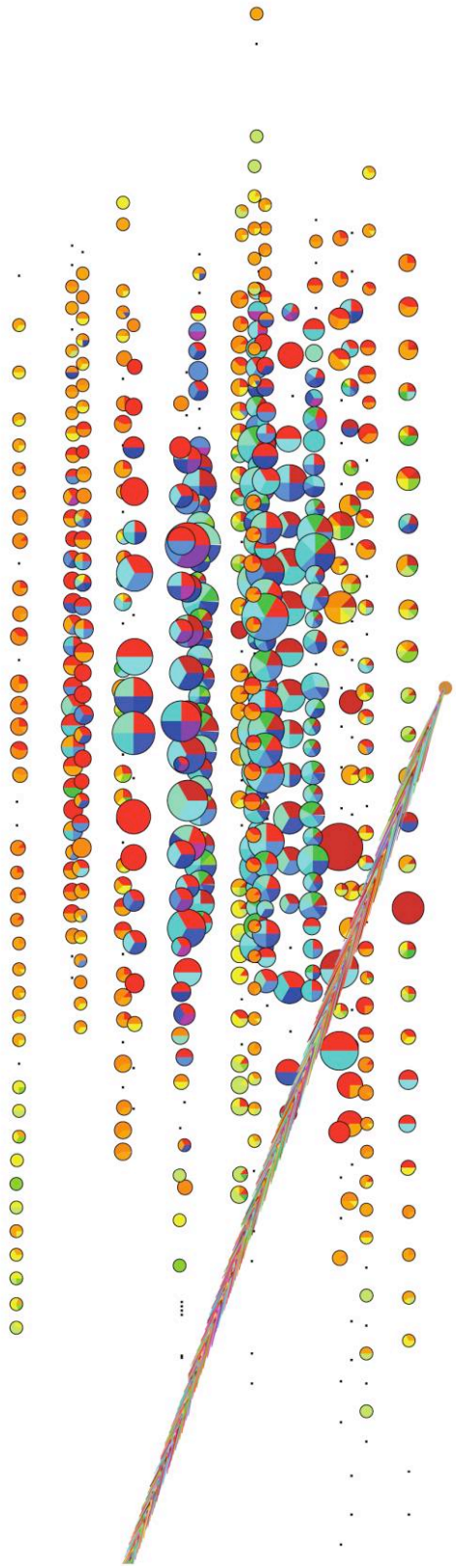


FIG. 1.—Simulated muon neutrino event with an energy of 3.8×10^8 GeV. The muon passes roughly 70 m outside the instrumented volume of the detector. Colored circles represent hit OMs. The color of the circle indicates the hit time (red is earliest), with multiple colors indicating multiple hits in that OM. The size of the circle is correlated with the number of photons produced.

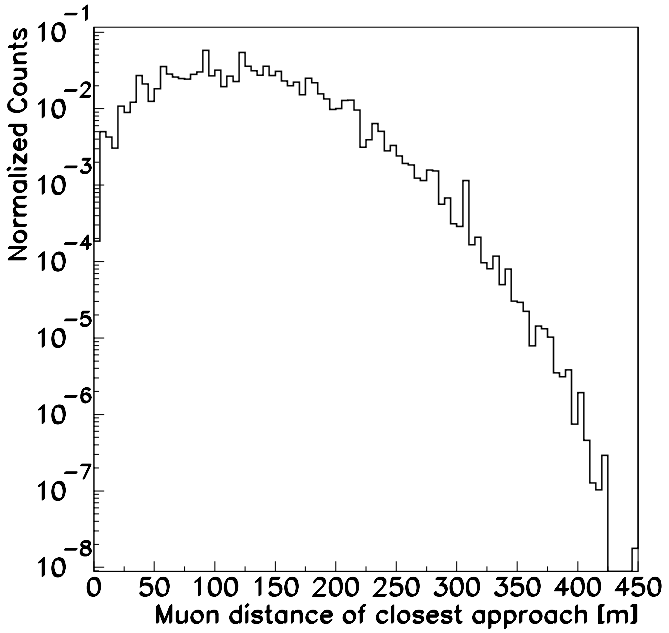


FIG. 2.—Distance of closest approach to the detector center for muons from UHE muon neutrinos (shown with an E^{-2} spectrum) that pass all selection criteria of this analysis.

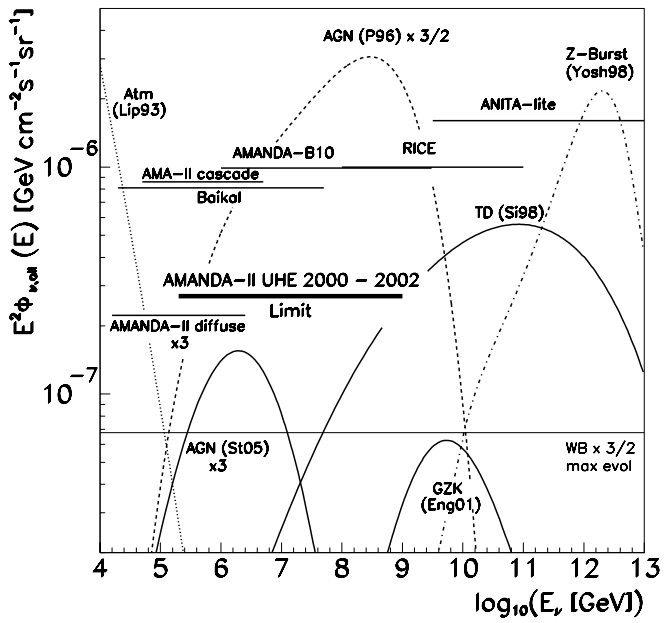


FIG. 3.—All-flavor UHE neutrino flux limit for 2000–2002 over the range that contains the central 90% of the expected signal with an E^{-2} spectrum. Also shown are several representative models: St05 from Stecker (2005) multiplied by 3, P96 from Protheroe (1997) multiplied by 3/2, Eng01 from Engel et al. (2001; curve shown for $\Lambda = 0.7$, taken from ftp://ftp.bartol.udel.edu/seckel/ess-gzk/flux_n3_8_flat_om0p3.txt.), Si98 from Sigl et al. (1998), Yosh98 from Yoshida et al. (1998), Lip93 from Lipari (1993), and the Waxman-Bahcall upper bound (Bahcall & Waxman 1998) multiplied by 3/2. Existing experimental limits shown are from the RICE (Kravchenko et al. 2006), ANITA-lite (Barwick et al. 2006), and Baikal (Aynutdinov et al. 2006) experiments, the UHE limit from AMANDA-B10 (Ackermann et al. 2005), the lower energy diffuse muon limit multiplied by 3 (Achterberg et al. 2007), and the cascade limit (Ackermann et al. 2004) from AMANDA-II.

well as the leading edge time and time over threshold for each hit, with each OM recording a maximum of eight hits per event. Each photoelectron has approximately a 3% chance of producing an afterpulse caused by ionization of residual gas inside the PMT (Hamamatsu 1999). This afterpulse follows several microseconds after the generating hit and aids in the detection of UHE events.

AMANDA-II has been collecting data since 2000 February. In 2002/2003, waveform digitizers were installed that record the full pulse shape from each OM (Silvestri 2005). In 2005 deployment began on IceCube (Ahrens et al. 2004b), a 1 km^3 array of digital OMs that now encompasses the AMANDA-II detector.

3. ASTROPHYSICAL NEUTRINO AND BACKGROUND SOURCES

Astrophysical neutrinos with energies in excess of 10^5 GeV may be produced by a variety of sources. A number of theories predict neutrino fluxes from active galactic nuclei (AGNs) peaking near 10^6 GeV. In these scenarios, protons are accelerated by the first-order Fermi mechanism in shock fronts. In the favored mechanism for neutrino production, these protons interact with the ambient photon field in either the cores (Stecker et al. 1992) or jets (Protheroe 1997; Halzen & Zas 1997; Mannheim et al. 2000; Mannheim 1995) of the AGN and produce neutrinos via the process

$$p + \gamma \rightarrow \Delta^+ \rightarrow \pi^+(+n) \rightarrow \nu_\mu + \mu^+ \rightarrow \nu_\mu + e^+ + \nu_e + \overline{\nu}_\mu, \quad (1)$$

resulting in a $\nu_e : \nu_\mu : \nu_\tau$ flavor ratio of 1:2:0 at the source.[40] The energy spectrum of the neutrinos produced by these interactions generally follows the E^{-2} spectrum of the protons. Theoretical bounds can be placed on the flux of these neutrinos based on the observation of cosmic rays if the p-γ reaction takes place in the jet or other optically thin region of the AGN (Bahcall & Waxman 1998; Mannheim et al. 2000).

UHE neutrinos are also associated with models created to explain the apparent excess of cosmic rays at the highest energies. One scenario involves the decay of massive objects, such as topological defects created by symmetry breaking in the early universe (Sigl et al. 1998). These objects decay close to the Earth into showers of particles, eventually producing neutrinos, as well as a fraction of the highest energy cosmic rays. Z-burst models could also produce some of the highest energy cosmic rays through the interaction of neutrinos with energies in excess of 10^{13} GeV with relic neutrinos via the Z^0 resonance. Since these neutrino-neutrino interactions are rare, it is possible to directly search for the UHE neutrino fluxes required by this mechanism (Yoshida et al. 1998; Kalashev et al. 2002a). It should be noted that Z-burst scenarios that predict the highest flux of neutrinos have already been eliminated by previous experiments (Barwick et al. 2006). In addition, Z-burst models predict fluxes of neutrinos that peak at energies above the sensitivity of this analysis or require unrealistic assumptions and are mentioned primarily for completeness.

A guaranteed source of UHE neutrinos comes from the interaction of high-energy cosmic rays with the cosmic microwave background (see, e.g., Engel et al. 2001 and Kalashev et al. 2002b). However, the flux predictions of these Greisen-Zatsepin-Kuzmin (GZK) neutrinos are generally several orders of magnitude lower than most of the fluxes listed previously.

[40] Neutrino flavor oscillation changes the flavor ratio to 1:1:1 at the Earth. See Kashti & Waxman (2005) for a discussion of different flavor ratios.

TABLE 1
Selection Criteria

Level	Selection Criteria	
0	Hit cleaning and retriggering	
1	F1H < 0.72, NHITS > 140	
2	F1H < 0.53	
	Cascade-like	Muon-like
3	$L_{\rm casc} < 7$, neural net > 0.93	$L_{\rm casc} \geq 7$, zenith angle > 85
4	F4H < 0.1	$L_{\rm muon} < 6.9$
5	$\rm F1H_{ELEC} < 0.56$	...
6	$L_{60} < 6.6$	...

The background for this analysis consists of bundles of muons from cosmic rays. The cosmic rays follow an $E^{-2.7}$ spectrum until about 10^6 GeV, where the flux steepens to E^{-3} (Hörandel 2003). They come only from the Southern Hemisphere because bundles from other directions are absorbed by the Earth. According to simulations, there can be as many as 20,000 muons in one bundle spread over a rms cross-sectional area as large as 200 m^2, and the highest energy events can deposit energies as large as 2.4×10^6 GeV in the ice around the AMANDA-II detector.

4. SIMULATION AND EXPERIMENTAL DATA

UHE neutrinos are simulated using the All Neutrino Interaction Simulation (ANIS) package (Kowalski & Gazizov 2005) to generate and propagate the neutrinos through the Earth. All three flavors of neutrinos are simulated with energies between 10^3 and 10^{12} GeV. The resulting muons and taus are propagated through the rock and ice near the detector using the Muon Monte Carlo (MMC) simulation package (Chirkin & Rhode 2004). Finally, the detector response is simulated using the AMASIM2 simulation package (Hundertmark 1999).

The background muon bundles from cosmic rays are generated using the CORSIKA simulation program with the QGSJET01 hadronic interaction model (Heck 1999). At early levels of this analysis, cosmic-ray primaries are generated with composition and spectral indices from Wiebel-Sooth et al. (1999) with energies of the primary particles ranging between 8×10^2 and 10^{11} GeV. At later levels of this analysis, the lower energy primaries have been removed by the selection criteria, and a new simulated data set is used with energy, spectral shape, and composition optimized to simulate high-energy cosmic rays more efficiently. In this optimized simulation, the energy threshold is raised to 8×10^4 GeV and only proton and iron primaries are generated with a spectrum of E^{-2}. These primaries are reweighted following the method outlined in Glasstetter et al. (1999). This optimized simulation is used for level 2 of the analysis and beyond (see Table 1). For 2001 and 2002, the background simulation is further supplemented with the inclusion of a third set of simulated data with the energy threshold increased to 10^6 GeV. For all sets of background simulation, the resulting particles are propagated through the ice using MMC, and the detector response is simulated using AMASIM2.

Data used in this analysis were recorded in the time period between 2000 February and 2002 November, with breaks each austral summer for detector maintenance, engineering, and calibration lasting approximately 4 months. In addition to maintenance downtime, the detector also has a brief period while recording each event in which it cannot record new events. Runs with anomalous characteristics (such as excessive trigger rates or large numbers of OMs not functioning) are discarded, and a method that removes nonphysical events caused by short-term detector instabilities is

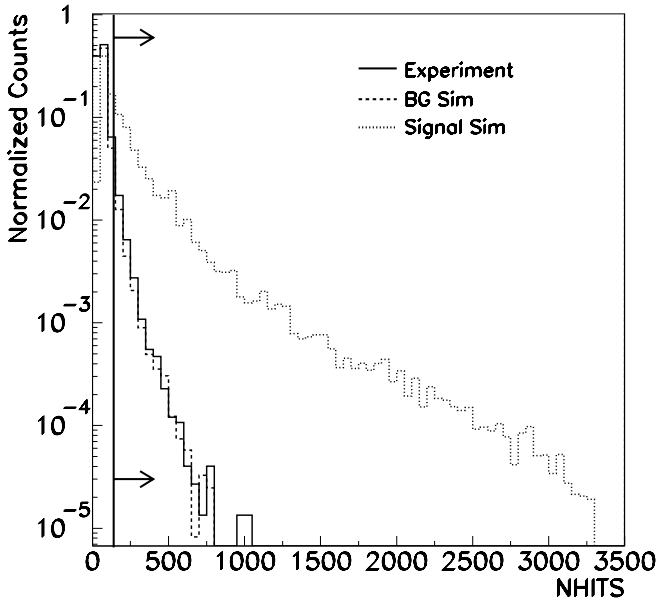


FIG. 4.—NHITS distribution for the experiment, background, and E^{-2} muon neutrino signal simulations before level 1 of this analysis.

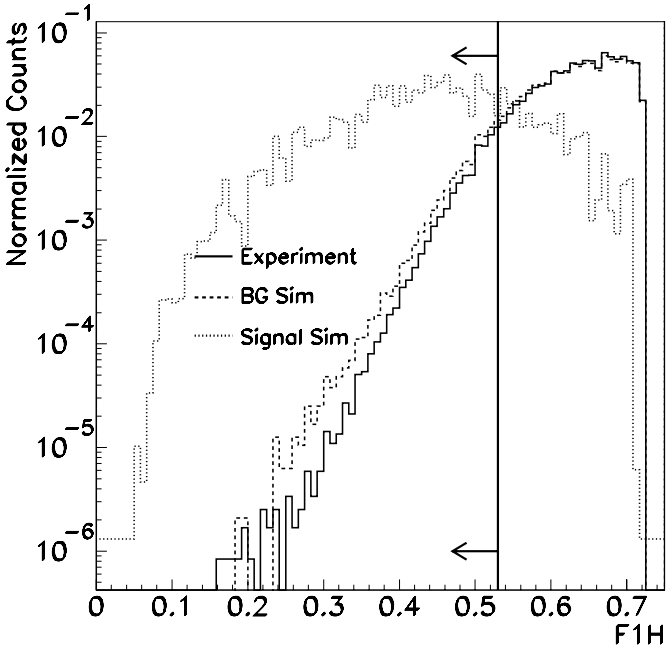


FIG. 5.—Distribution of F1H (the fraction of OMs with a single hit) for the experiment, background, and E^{-2} muon neutrino signal simulations after level 1 of this analysis. The average F1H drops with energy (see Fig. 6).

applied (Pohl 2004). These factors combine to give a dead time of 17% of the data-taking time for 2000, 22% of the data-taking time for 2001, and 15% of the data-taking time for 2002. In addition, 26 days are excluded from 2000 because the UHE filtered events are polluted with a high number of events with incomplete hit information, likely due to a minor detector malfunction. Taking these factors into account, there are 173.5 days of live time in 2000, 192.5 days of live time in 2001, and 205.0 days of live time in 2002. Finally, 20% of the data from each year is set aside for comparison with simulations and to aid in the determination of selection criteria, leading to a total live time for the 3 yr of 456.8 days.

5. ANALYSIS

Twenty percent of the data from 2000 to 2002 (randomly selected from throughout the 3 yr) is used to test the agreement between background simulations and observations. In order to avoid biasing the determination of selection criteria, this 20% is then discarded, and the developed selection criteria are applied to the remaining 80% of the data. A previous UHE analysis was performed on only the 2000 data using different selection criteria than those described below (see Gerhardt 2005, 2007 for a more detailed description). For 2001–2002, improved reconstruction techniques such as cascade reconstructions (Ahrens et al. 2003c) were added to the analysis, and the new selection criteria described below were devised in a blind manner. These selection criteria were also applied to the 2000 data to derive a combined 3 yr limit. Due to differences in hit selection for reconstruction between 2000 and 2001–2002, the E^{-2} signal passing rate at the final selection level for the year 2000 is approximately 60% of the rate for the years 2001 and 2002.

In order to maximize the limit-setting potential, the selection criteria are initially determined by optimizing the model rejection factor (MRF; Hill & Rawlins 2003) given by

$$\mathrm{MRF} = \frac{\bar{\mu}_{90}}{N_{\mathrm{signal}}}, \tag{2}$$

where $\bar{\mu}_{90}$ is the 90% confidence level (CL) average event upper limit given by Feldman & Cousins (1998) and N_{signal} is the number of muon neutrinos expected for the signal being tested, in this case an E^{-2} flux. The selection criteria for this analysis are summarized in Table 1 and described below.

This analysis exploits the differences in total energy and light deposition between bundles of many low-energy muons and single UHE muons or cascades from UHE neutrinos. UHE neutrinos deposit equal or greater amounts of light in the ice than background muon bundles. In addition to being lower energy, background muon bundles spread their light over the cross-sectional area of the entire muon bundle, rather than just along a single muon track or into a single cascade. Both signal and background events can have a large number of hits in the array, but for the same number of hit OMs, the muon bundle has a lower total number of hits, NHITS (recall that each OM may have multiple separate hits in one event; see Fig. 4). The number of hits for UHE neutrinos is increased by the tendency of bright signals to produce afterpulses in the PMT. Background muon bundles also have a higher fraction of OMs with a single hit (F1H), while a UHE neutrino generates more multiple hits (Fig. 5). The F1H variable is correlated with energy (Fig. 6) and is effective at removing lower energy background muon bundle events. The level 1 and 2 selection criteria require that NHITS > 140 and F1H < 0.53 and reduce the background by a factor of 2×10^3 relative to trigger level (level 0 on Tables 2 and 3).

At this point the data sample is sufficiently reduced that computationally intensive reconstructions become feasible. Reconstruction algorithms used in this analysis employ a maximum likelihood method that takes into account the absorption and scattering of light in ice. For muons, the reconstruction compares time residuals to those expected from a Cerenkov cone for a minimally ionizing muon (Ahrens et al. 2004a), while the cascade reconstruction uses Cerenkov light from an electromagnetic cascade for comparison (Ahrens et al. 2003c). Reconstructions that are optimized for spherical (cascade) depositions of light are used to distinguish UHE neutrinos from background muon bundles that happen to have a large energy deposition, such as a bremsstrahlung or e^+-e^- pair creation, inside the detector fiducial volume.

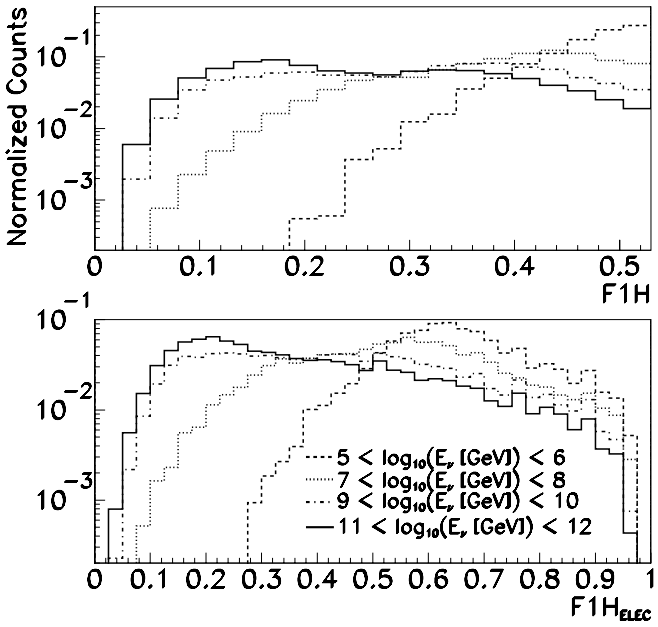


FIG. 6.—F1H (*top*) and $F1H_{ELEC}$ (*bottom*) distributions for various energy decades of muon neutrino signal. These variables serve as a rough estimator of energy for the UHE analysis.

Before application of the level 3 selection criteria, the data sets are split into "cascade-like" and "muon-like" subsets. This selection is performed using the negative log likelihood of the cascade reconstruction (L_{casc}; see Fig. 7), where events with a $L_{casc} < 7$ are considered cascade-like.

5.1. *"Cascade-like" Events*

Background events in the cascade-like subset are characterized by either a large light deposition in or very near the instrumented volume of AMANDA-II or a path that clips the top or bottom of the array. In either case, the energy deposition is significantly less than the energy deposited by a UHE neutrino, allowing the application of selection criteria that correlate with energy. One of these is $F1H_{ELEC}$ (Fig. 8), a variable similar to the F1H variable described above, except that it uses only OMs whose signal is brought to the surface by electrical cables. The signal spreads as it propagates up the cable, causing hits close together in time to be combined. This gives $F1H_{ELEC}$ a different distribution from F1H, and both variables are good estimators of energy deposited inside the detector (Fig. 6). In addition, the fraction of OMs with exactly four hits (F4H) is another useful energy indicator. The value of four hits was chosen as a compromise between the number of hits expected from OMs with electrical cables and OMs with optical fibers. OMs with optical fibers typically have more hits than OMs with electrical cables because very little pulse spreading occurs as the signal propagates up the fiber. The level 3 selection criteria use the output of a neural net with $F1H_{ELEC}$, F4H, and F1H as input variables (Fig. 9). As selection levels 4 and 5, separate applications of the F4H and $F1H_{ELEC}$ variables remove persistent lower energy background events.

The remaining background muon bundles have a different hit distribution than UHE neutrinos. In the background muon bundles, a large light deposition can be washed out by the continuous, dimmer light deposition from hundreds to tens of thousands of muon tracks. In contrast, UHE muons can have one light deposition that is several orders of magnitude brighter than the light from the rest of the muon track and looks very similar to bright cascades from UHE electron and tau neutrinos. For all cases, the

TABLE 2

NUMBER OF EXPERIMENTAL, SIMULATED BACKGROUND, AND SIMULATED SIGNAL EVENTS IN THE CASCADE-LIKE SUBSET AT EACH SELECTION LEVEL FOR 456.8 DAYS

Level	Data	BG Simulation	Signal Simulation
0	2.7×10^9	$1.8^{+1.8}_{-1.1} \times 10^9$	621.7
1	3.9×10^7	$3.1^{+3.1}_{-1.8} \times 10^7$	270.8
2	1.7×10^4	$1.4^{+1.4}_{-0.8} \times 10^4$	89.2
3	155	62^{+63}_{-37}	32.0
4	151	61^{+62}_{-37}	31.0
5	46	32^{+32}_{-19}	27.1
6	0	$0^{+2.6}$	16.0

NOTES.—Levels 0 and 1 show combined numbers for both muon-like and cascade-like subsets. Signal is shown with a low-energy threshold of 10^4 GeV for a neutrino spectrum of $dN/dE = 10^{-6}E^{-2}$ GeV^{-1} cm^{-2} s^{-1} sr^{-1}, with an assumed 1:1:1 $\nu_e : \nu_\mu : \nu_\tau$ flavor ratio. Values at selection levels 0 and 1 for data and background simulation are extrapolated from the 2000 data sets. The background simulation is shown with systematic and statistical uncertainties described in § 6. The numbers of muon-like events are shown in Table 3.

TABLE 3

NUMBER OF EXPERIMENTAL, SIMULATED BACKGROUND, AND SIMULATED SIGNAL EVENTS IN THE MUON-LIKE SUBSET AT EACH SELECTION LEVEL FOR 456.8 DAYS

Level	Data	BG Simulation	Signal Simulation
0	2.7×10^9	$1.8^{+1.8}_{-1.1} \times 10^9$	621.7
1	3.9×10^7	$3.1^{+3.1}_{-1.8} \times 10^7$	270.8
2	1.4×10^6	$9.0^{+9.1}_{-5.4} \times 10^5$	85.2
3	4.6×10^4	$2.7^{+2.7}_{-1.6} \times 10^4$	57.9
4	2	$0^{+2.6}$	4.0

NOTES.—Levels 0 and 1 show combined numbers for both muon-like and cascade-like subsets. Signal is shown with a low-energy threshold of 10^4 GeV for a neutrino spectrum of $dN/dE = 10^{-6}E^{-2}$ GeV^{-1} cm^{-2} s^{-1} sr^{-1}, with an assumed 1:1:1 $\nu_e : \nu_\mu : \nu_\tau$ flavor ratio. Values at selection levels 0 and 1 for data and background simulation are extrapolated from the 2000 data sets. The background simulation is shown with systematic and statistical uncertainties described in § 6. The numbers of cascade-like events are shown in Table 2.

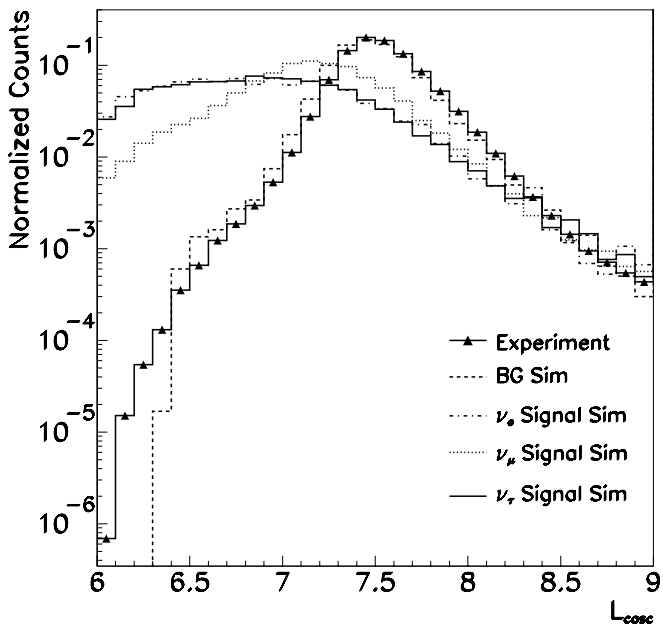


FIG. 7.—Distribution of L_{casc} for the experiment, background, and E^{-2} electron, muon, and tau neutrino signal simulations after level 2 of this analysis. Events with $L_{casc} < 7$ are "cascade-like," and events with $L_{casc} \geq 7$ are "muon-like."

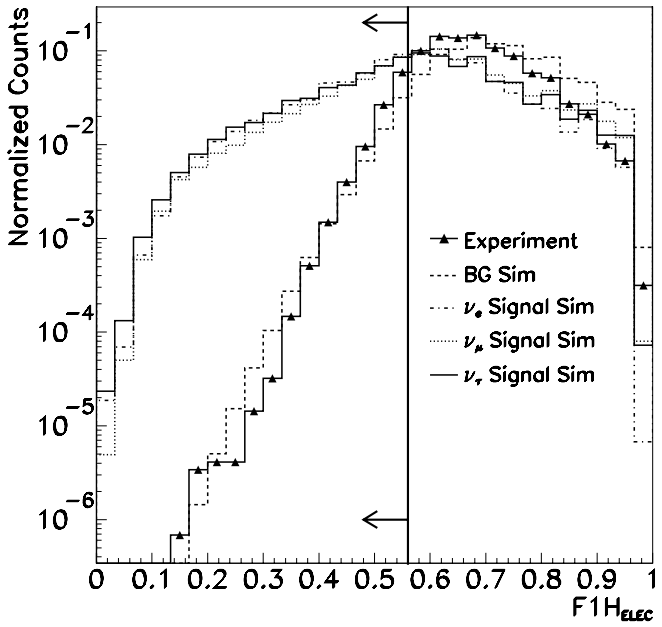


FIG. 8.—F1H$_{ELEC}$ (the fraction of electrical OMs with a single hit) distribution for the experiment, background, and E^{-2} electron, muon, and tau neutrino signal simulations in the cascade-like subset after level 2 of this analysis.

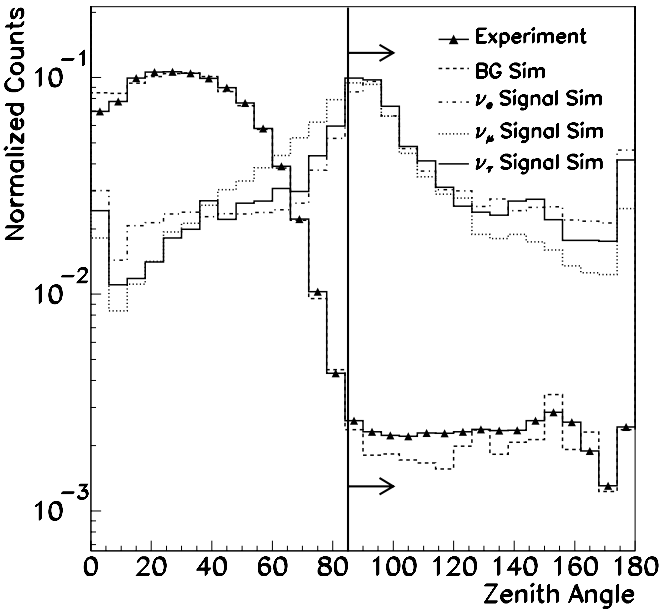


FIG. 10.—Reconstructed zenith angle distribution for the experiment, background, and E^{-2} electron, muon, and tau neutrino signal simulations in the muon-like subset after level 2 of this analysis. Zenith angles of 90° correspond to horizontal events, and zenith angles of 0° are downgoing events.

initial cascade reconstruction is generally concentric with this large energy deposition, so ignoring OMs that are within 60 m of the initial cascade reconstruction reduces the fraction of OMs that are triggered with photons from the cascade. For background, the remaining light will be dominated by light depositions from the tracks of the muon bundles and be less likely to reconstruct as a cascade. In contrast, signal events, with their energetic cascades, will still appear cascade-like and reconstruct with a better likelihood (L_{60}). The final selection criterion for cascadelike events (chosen by optimizing the MRF) requires that these events be well reconstructed by a cascade reconstruction performed using only OMs with distances greater than 60 m and reduces the background expectation to 0 events for this subset. The numbers of events at each selection level for experiment, background, and signal simulation for the cascade-like subset are shown in Table 2.

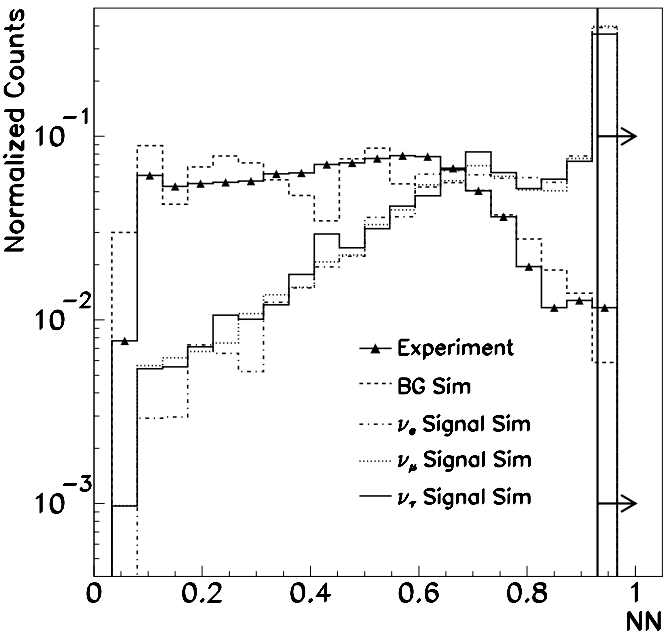


FIG. 9.—Distribution of neural net output for the experiment, background, and E^{-2} electron, muon, and tau neutrino signal simulations in the cascade-like subset after level 2 of this analysis. Signal events are expected near 1, while background events are expected near 0.

5.2. *"Muon-like" Events*

Background events in the muon-like subset are characterized by more uniform, tracklike light deposition and are more easily reconstructed by existing reconstruction algorithms than cascade-like events. A reconstruction algorithm based on parameterization of time residuals from simulated muon bundles is used to reconstruct the zenith angle of the events (Fig. 10). Since most background muon bundles will come from a downgoing direction, while UHE neutrinos will come primarily from the horizontal direction (Klein & Mann 1999), requiring that the zenith angle >85° (where a zenith angle of 90° is horizontal) reduces the background by a factor of 30. The remaining background in the muon-like subset are misreconstructed events, since the actual flux close to the horizon is very small. A reconstruction based on the hit pattern of a Cerenkov cone for a minimally ionizing muon is applied to these events (Ahrens et al. 2004a). Selecting only well-reconstructed events using the likelihood of this reconstruction ($L_{\rm muon}$) is sufficient to remove all background events in this subset. The value of this selection criterion was initially chosen to optimize the MRF for muon neutrinos with an E^{-2} spectrum. However, by increasing the selection value slightly beyond the value that gave the minimum MRF, all background events were rejected with only a few percent drop in the sensitivity (Fig. 11). Since the uncertainty in the cosmic-ray spectrum is very large at these energies, the more stringent selection criterion was applied to correct for the fact that the MRF is optimized without uncertainties. The numbers of events at each selection level for experiment, background, and signal simulation for the muon-like subset are shown in Table 3.

6. STATISTICAL AND SYSTEMATIC UNCERTAINTIES

Because there is no test beam that can be used to determine the absolute sensitivity of the AMANDA-II detector, calculations of

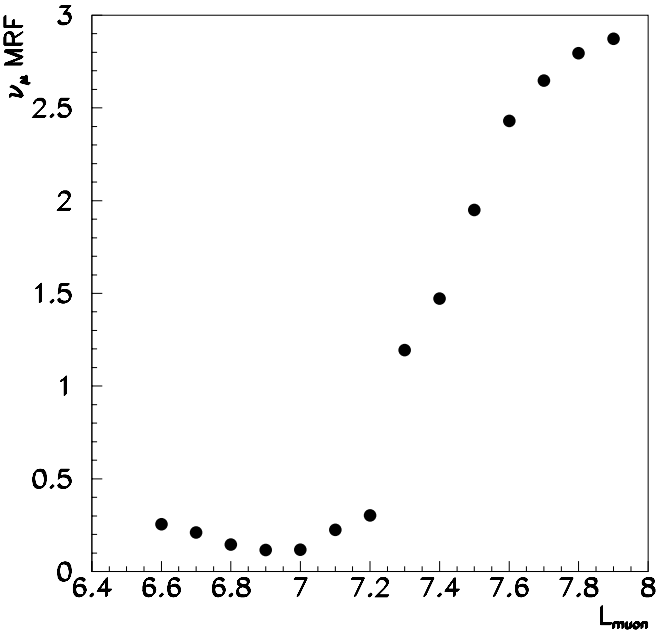


FIG. 11.—Model rejection factor for $10^{-6}E^{-2}$ muon neutrinos in the muon-like subset as a function of cut level for L_{muon}.

sensitivity rely on simulation. The dominant sources of statistical and systematic uncertainty in this calculation are described below. The systematic uncertainties are assumed to have a flat distribution and are summed in quadrature separately for background and signal. The uncertainties have been included into the final limit using the method described in Tegenfeldt & Conrad (2005).

6.1. *Uncertainties Due to Limited Simulation Statistics*

Due to computational requirements, background simulation statistics are somewhat limited. Ideally, one would scale the statistical uncertainty on zero events based on the simulation event weights in nearby nonzero bins. However, the optimized background simulations used in this analysis have large variations in event weights approaching this region, making determination of this factor difficult. Nevertheless, the statistical uncertainties near the edge of the distribution are on the order of the uncertainties for a simulation with a live time equivalent to the data-taking period, so no scaling factor is applied to the statistical uncertainty. A statistical uncertainty of 1.29, the 1 σ Feldman-Cousins event upper limit on zero observed events (Feldman & Cousins 1998), is assumed at the final selection level. Signal simulation has an average statistical uncertainty of 5% for each neutrino flavor.

6.2. *Normalization of Cosmic-Ray Flux*

The average energy of cosmic-ray primaries at the penultimate selection level is 4.4×10^7 GeV, which is considerably above the knee in the all-particle cosmic-ray spectrum. Numerous experiments have measured a large spread in the absolute normalization of the flux of cosmic rays at this energy (see Kampert 2007 for a recent review). Estimates of the uncertainty in the normalization of the cosmic-ray flux range from 20% (Hörandel 2003) to a factor of 2 (Particle Data Group 2006). This analysis uses the more conservative uncertainty of a factor of 2.

6.3. *Cosmic-Ray Composition*

There is considerable uncertainty in the cosmic-ray composition above the knee (Particle Data Group 2006). We estimate the systematic uncertainty by considering two cases: proton-dominated composition and iron-dominated composition. The simulated background cosmic-ray flux is approximated by separately treating proton and iron primaries combined in a total spectrum that becomes effectively iron dominated above 10^7 GeV using the method described in Glasstetter et al. (1999). The iron-dominated spectrum yields a 30% higher background event rate than the rate from a proton-dominated spectrum at the penultimate selection level. This value of 30% is used as the uncertainty due to the cosmic-ray composition.

6.4. *Detector Sensitivity*

The properties of the refrozen ice around each OM, the absolute sensitivity of individual OMs, and obscuration of OMs by nearby power cables can affect the detector sensitivity. This analysis uses the value obtained in Ahrens et al. (2003a), where reasonable variations of these parameters in the simulation were found to cause a 15% variation in the E^{-2} signal and background passing rate.

6.5. *Implementation of Ice Properties*

As photons travel through the ice they are scattered and absorbed. The absorption and scattering lengths of the ice around the AMANDA-II detector have been measured very accurately using in situ light sources (Ackermann et al. 2006). Uncertainties are introduced due to the limited precision with which these parameters are included in the simulation. Varying the scattering and absorption lengths in the detector simulation by 10% was found to cause a difference in the number of expected signal events (for an E^{-2} spectrum) of 34% (Ackermann et al. 2005), which is used as a conservative estimate of the uncertainty due to implementation of ice properties. If too large of a deviation in background rate relative to the experimental rate was observed for a set of ice property parameters, the background rate was normalized to the experimental rate, and the signal rate was scaled accordingly. This was done to ensure that the variation in absorption and scattering lengths covered a reasonable range of ice properties.

6.6. *Neutrino Cross Section*

The uncertainty in the standard model neutrino cross section has been quantified recently (Anchordoqui et al. 2006), taking into account the experimental uncertainties on the parton distribution functions measured at HERA (Chekanov et al. 2005), as well as theoretical uncertainties in the effect of heavy quark masses on the parton distribution function evolution and on the calculation of the structure functions. The corresponding maximum variation in the number of expected signal events (for an E^{-2} spectrum) is 10%, in agreement with previous estimates (Ackermann et al. 2005).

Screening effects are expected to suppress the neutrino-nucleon cross section at energies in excess of 10^8 GeV (see, e.g., Kutak & Kwiecinski 2003; Berger et al. 2007). This has a negligible effect on the number of signal events expected for an E^{-2} spectrum because the majority of signal is found below these energies (Fig. 12). Even if the suppression is as extreme as in the color glass condensate model (Henley & Jalilian-Marian 2006), the event rate decreases by only 11%.

6.7. *Differences in Simulated Distributions*

An examination of the L_{muon} distribution for the muon-like subset after level 3 of this analysis suggests that the background simulation is shifted by one bin relative to the experiment (Fig. 13).

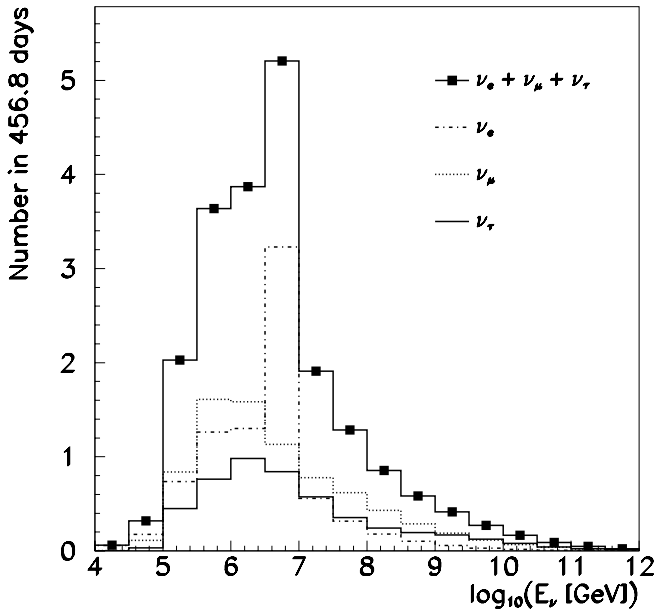


FIG. 12.—Energy spectra of electron, muon, and tau neutrino signal events $[d(N_{\nu_e} + N_{\nu_\mu} + N_{\nu_\tau})/dE = 10^{-6}E^{-2}$ GeV $^{-1}$ cm^{-2} s^{-1} sr^{-1}] that pass all selection criteria. The peak in the electron neutrino spectrum just below 10^7 GeV is due to the Glashow resonance.

Shifting all simulation distributions to the left by one bin leads to better agreement between the background simulation and experimental distributions and an increase in 8% in the number of expected signal events for an E^{-2} spectrum.

6.8. *The Landau-Pomeranchuk-Migdal* (*LPM*) *Effect*

At ultrahigh energies, the LPM effect suppresses the bremsstrahlung cross section for electrons and the pair production cross section of photons created in a cascade by an electron neutrino (Landau & Pomeranchuk 1953; Migdal 1957). This lengthens the resulting shower produced by a factor that goes as $\sqrt{E}$. Above

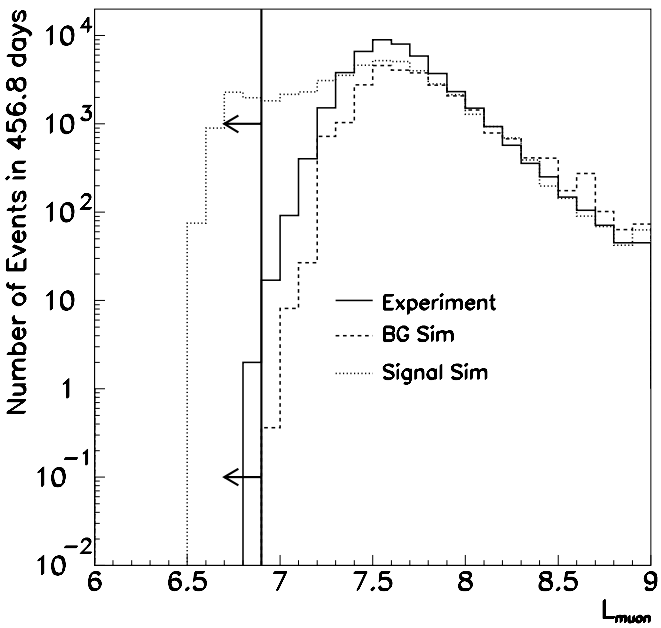


FIG. 13.—The $L_{\rm muon}$ distribution for the experiment, background, and $4.5 \times 10^{-4}E^{-2}$ muon neutrino signal simulations (arbitrary normalization) in the muon-like subset after level 3 of this analysis. Two experimental events survive the final selection criteria of $L_{\rm muon} < 6.9$.

TABLE 4
SIMULATION UNCERTAINTIES

Source	Background Simulation (%)	Signal Simulation (%)
Cosmic-ray normalization	+100/−50	...
Cosmic-ray composition	−30	...
Detector sensitivity	±15	±15
Ice properties	...	±34
Neutrino cross section	...	±10
Simulation distribution	...	+8
LPM effect	...	−2
Total	+101/−60	+39/−39

10^8 GeV, the extended shower length becomes comparable to the spacing between OMs on a string (Klein 2004). In addition, as the LPM effect suppresses the bremsstrahlung and pair production's cross sections, photonuclear and electronuclear interactions begin to dominate, which lead to the production of muons inside the electromagnetic cascade. Toy simulations were performed that superimposed a muon with an energy of 10^5 GeV onto a cascade with energy of 10^8 GeV. While the addition of the muon shifted the $L_{\rm casc}$ distribution 5% toward higher (more muon-like) values, the resulting events still passed all selection criteria, indicating that the effects of muons created inside cascades are negligible.

The LPM effect is not included in the simulations of electron neutrinos, but it can be approximated by excluding all electron neutrinos with energies in excess of 10^8 GeV. This is an overestimation of the uncertainty introduced by the LPM effect, as extended showers may manifest as several separate showers that are likely to survive all selection criteria and the addition of low-energy muons is not expected to significantly alter the UHE cascade light deposition. Neglecting electron neutrinos with energies in excess of 10^8 GeV reduces the number of expected signal events by 2% for an E^{-2} spectrum.

6.9. *Summary of Uncertainties*

The systematic errors are shown in Table 4. Summing the systematic errors of the signal simulation in quadrature gives a systematic uncertainty of ±39%. Combining this with the statistical uncertainty of 5% per neutrino flavor gives a total maximum uncertainty of 40%. Following a similar method for the background simulation, the systematic uncertainty is +101%/−60%. Scaling the statistical uncertainty of the background simulation by the systematic uncertainty gives a maximum background expectation of fewer than 2.6 events for 3 yr.

7. RESULTS

After applying all selection criteria, no background events are expected for 456.8 days. Incorporating the statistical and systematic uncertainties, the background is expected to be found with a uniform prior probability between 0 and 2.6 events. A possible sensitivity calculation that incorporates these uncertainties can be generated by assuming a flat prior with a mean of 1.3 events and a corresponding data expectation of 1 event. This gives a 90% CL event upper limit of 3.5 (Tegenfeldt & Conrad 2005) and a sensitivity of 1.8×10^{-7} GeV cm^{-2} s^{-1} sr^{-1}, with the central 90% of the E^{-2} signal found in the energy range 2×10^5 to 10^9 GeV. Table 5 shows the expected number of each flavor of UHE neutrino passing the final selection level for a $10^{-6}E^{-2}$ flux. The energy spectra of each flavor are shown in Figure 12.

TABLE 5

NUMBER OF SIMULATED NEUTRINO EVENTS IN THE CASCADE-LIKE AND MUON-LIKE SUBSETS PASSING ALL SELECTION CRITERIA FOR 3 yr FOR A NEUTRINO SPECTRUM OF $d(N_{\nu_e} + N_{\nu_\mu} + N_{\nu_\tau})/dE = 10^{-6}E^{-2}$ GeV^{-1} cm^{-2} s^{-1} sr^{-1}

Neutrino Flavor	Cascade-like	Muon-like	Total
Electron	7.7	0.1	7.8
Muon	3.9	3.6	7.5
Tau	4.4	0.3	4.7
All flavors	16.0	4.0	20.0

Two events are observed in the data sample at the final selection level (Fig. 13), while fewer than 2.6 background events are expected, which gives a 90% CL average event upper limit of 5.3. After applying all selection criteria, 20 events are expected for a $10^{-6}E^{-2}$ all flavor flux (Table 5). The upper limit on the all-flavor neutrino flux (assuming a 1:1:1 $\nu_e:\nu_\mu:\nu_\tau$ flavor ratio) is

$$E^2\Phi_{90\%\mathrm{CL}} \leq 2.7\times10^{-7}\ \mathrm{GeV\ cm^{-2}\ s^{-1}\ sr^{-1}}, \qquad (3)$$

including systematic uncertainties, with the central 90% of the E^{-2} signal found between the energies of 2×10^5 and 10^9 GeV.

A number of theories that predict fluxes with non-E^{-2} spectral shapes (Fig. 3) were also tested by reweighting the simulated signal. These include the hidden-core AGN model of Stecker et al. (1992), which has been updated to reflect a better understanding of AGN emission (Stecker 2005), as well as AGN models in which neutrinos are accelerated in optically thin regions (Protheroe 1997; Halzen & Zas 1997; Mannheim 1995; Mannheim et al. 2000). Including uncertainties, this analysis restricts at a 90% CL the AGN models from Halzen & Zas (1997) and Mannheim et al. (2000). In addition, the previously rejected (Ackermann et al. 2005) models from Protheroe (1997) and Stecker et al. (1992) are rejected at the 90% CL by this analysis (see Fig. 14 and Table 6). The model by Stecker et al. (1992) builds on a correlation between X-rays and neutrinos from AGNs. Other models using the same correlation give a similar normalization and violate current limits by 1 order of magnitude as well. As previously pointed out by Becker et al. (2007), such a correlation can be excluded.

TABLE 6

FLUX MODELS, THE NUMBER OF NEUTRINOS OF ALL FLAVORS EXPECTED AT THE EARTH AT THE FINAL SELECTION LEVEL, AND THE MRFS FOR 456.8 DAYS OF LIVE TIME

Model	ν_{all}	MRF	Reference
AGN[a]	20.6	0.3	Protheroe (1997)
	17.4	0.3	Stecker et al. (1992)
	8.8	0.6	Halzen & Zas (1997)
	5.9	0.9	Mannheim et al. (2000)
AGN RL B[a]	4.5	1.2	Mannheim (1995)
Z-burst	2.0	2.7	Kalashev et al. (2002a)
AGN	1.8	2.9	Stecker (2005)
GZK ν norm AGASA[b]	1.8	2.9	Ahlers et al. (2005)
GZK ν monoenergetic	1.2	4.4	Kalashev et al. (2002b)
GZK ν $a = 2$	1.1	4.8	Kalashev et al. (2002b)
GZK ν norm HiRes[b]	1.0	5.3	Ahlers et al. (2005)
TD	0.9	5.9	Sigl et al. (1998)
AGN RL A[a]	0.3	18.0	Mannheim (1995)
Z-burst	0.1	53.0	Yoshida et al. (1998)
GZK ν	0.06	88.0	Engel et al. (2001)

NOTE.—A MRF of less than 1 indicates that the model is excluded with 90% confidence.

[a] These values have been divided by 2 to account for neutrino oscillation from a source with an initial 1:2:0 $\nu_e:\nu_\mu:\nu_\tau$ flux.

[b] Lower energy threshold of 10^7 GeV applied.

While we do not directly exclude the flux from the Stecker (2005) hidden-core AGN model, it is possible to set limits on the parameters used in the model. In this model, the flux of neutrinos is normalized to the extragalactic MeV photon flux measured by COMPTEL with the assumption that the flux of photons from Seyfert galaxies is responsible for 10% of this MeV background. If the neutrino flux scales linearly with the photon flux, then the maximum contribution of hidden-core AGNs, such as Seyfert

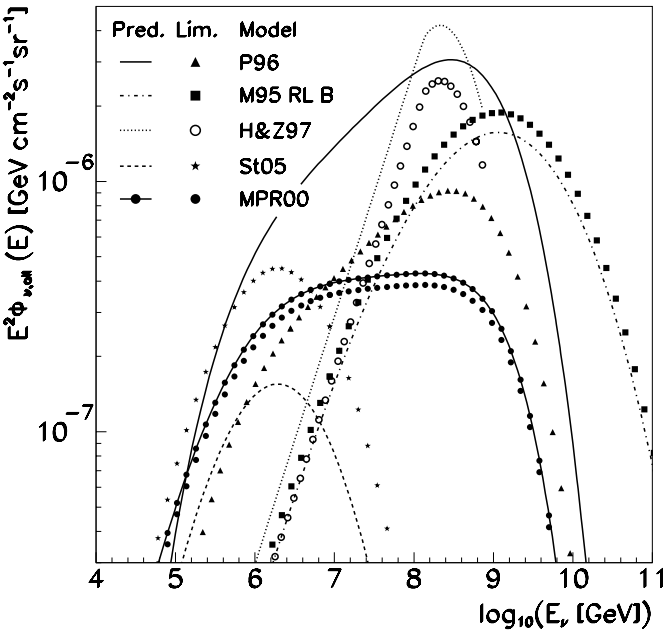


FIG. 14.—AGN fluxes tested in this paper. Lines denote the model predictions and symbols denote the 90% CL limits on the predictions derived by this analysis. The models rejected at the 90% CL shown are H&Z97 from Halzen & Zas (1997), P96 from Protheroe (1997), and MPR00 from Mannheim et al. (2000). Also shown are models close to being rejected: M95 RL B from Mannheim (1995) and St05 from Stecker (2005). See Table 6 for exact numbers.

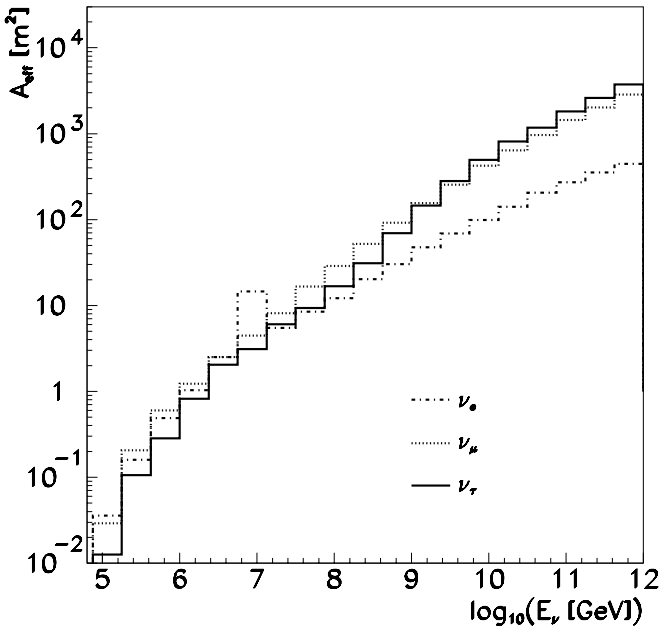


FIG. 15.—Angle-averaged neutrino effective area at final selection level as a function of neutrino energy for electron, muon, and tau neutrinos. The peak in the electron neutrino effective area just below 10^7 GeV is due to the Glashow resonance.

galaxies, to the extragalactic MeV photon flux must be less than 29%.

Fluxes of neutrinos from the decay of topological defects (Sigl et al. 1998) and the UHE fluxes required for the *Z*-bursts mechanism (Yoshida et al. 1998; Kalashev et al. 2002a) peak at too high of an energy to be detected by this analysis. Neutrinos from the interaction of cosmic rays with cosmic microwave background photons are produced at too low of a flux for this analysis to detect (see Table 6).

The number of expected events of a given flavor (ν and $\overline{\nu}$) for spectra not tested in this paper can be calculated using the formula

$$N_{\rm signal} = T \int dE_\nu \, d\Omega \Phi_\nu(E_\nu) A^\nu_{\rm eff}(E_\nu), \qquad (4)$$

where T is the total live time (456.8 days), $A^\nu_{\rm eff}$ is the angle-averaged neutrino effective area (Fig. 15), and Φ_ν is the flux at the Earth's surface.

8. CONCLUSION

The diffuse neutrino flux limit for a 1:1:1 $\nu_e:\nu_\mu:\nu_\tau$ flavor ratio set by this analysis of

$$E^2\Phi_{90\%\rm CL} \leq 2.7\times10^{-7}\ \rm GeV\ cm^{-2}\ s^{-1}\ sr^{-1} \qquad (5)$$

is the most stringent to date above 10^5 GeV. A number of models for neutrino production have been rejected (see Table 6 for a full list). AMANDA-II hardware upgrades that were completed in 2003 should lead to an improvement of the sensitivity at ultra-high energies (Silvestri 2005). In addition, AMANDA-II is now surrounded by the next-generation IceCube detector, which is currently under construction. The sensitivity to UHE muon neutrinos for 1 yr is expected to increase by roughly 1 order of magnitude as the IceCube detector approaches its final size of 1 km^3 (Ahrens et al. 2004b).

We acknowledge the support from the following agencies: National Science Foundation–Office of Polar Programs; National Science Foundation–Physics Division; University of Wisconsin Alumni Research Foundation; Department of Energy and National Energy Research Scientific Computing Center (supported by the Office of Energy Research of the Department of Energy); the NSF-supported TeraGrid system at the San Diego Supercomputer Center (SDSC); the National Center for Supercomputing Applications (NCSA); Swedish Research Council; Swedish Polar Research Secretariat; Knut and Alice Wallenberg Foundation, Sweden; German Ministry for Education and Research; Deutsche Forschungsgemeinschaft (DFG), Germany; Fund for Scientific Research (FNRS-FWO); Flanders Institute to encourage scientific and technological research in industry (IWT); Belgian Federal Office for Scientific, Technical and Cultural affairs (OSTC); and the Netherlands Organisation for Scientific Research (NWO). M. Ribordy acknowledges the support of the SNF (Switzerland); A. Kappes and J. D. Zornoza acknowledge the Marie Curie OIF Program; L. Gerhardt acknowledges the support of the University of California, Irvine MPC Computational Cluster and Achievement Rewards for College Scientists (ARCS).

REFERENCES

Achterberg, A., et al. 2007, Phys. Rev. D, 76, 042008
Ackermann, M., et al. 2004, Astropart. Phys., 22, 127
———. 2005, Astropart. Phys., 22, 339
———. 2006, J. Geophys. Res., 3, D13203
Ahlers, M., et al. 2005, Phys. Rev. D, 72, 023001
Ahrens, J., et al. 2003a, ApJ, 583, 1040
———. 2003b, Phys. Rev. Lett., 90, 251101
———. 2003c, Phys. Rev. D, 67, 012003
———. 2004a, Nucl. Instrum. Methods A, 524, 169
———. 2004b, Astropart. Phys., 20, 507
Anchordoqui, L., Cooper-Sakar, A., Hooper, D., & Sakar, S. 2006, Phys. Rev. D, 74, 043008
Aynutdinov, V., et al. 2006, Astropart. Phys., 25, 140
Bahcall, J., & Waxman, E. 1998, Phys. Rev. D, 59, 023002
Barwick, S., et al. 2006, Phys. Rev. Lett., 96, 171101
Becker, J. K., Groß, A., Münich, K., Dreyer, J., Rhode, W., & Biermann, P. L. 2007, Astropart. Phys., 28, 98
Berger, E., Block, M., McKay, D., & Tan, C. 2007, preprint (hep-ph/0708.1960v1)
Chekanov, S., et al. 2005, European J. Phys. C, 42, 1
Chirkin, D., & Rhode, W. 2004, preprint (hep-ph/0407075)
Engel, R., Seckel, D., & Stanev, T. 2001, Phys. Rev. D, 64, 093010
Feldman, G., & Cousins, F. 1998, Phys. Rev. D, 57, 3873
Gandhi, R., Quigg, C., Reno, M., & Sarcevic, I. 1998, Phys. Rev. D, 58, 093009
Gerhardt, L. 2005, in Proc. 29th Int. Cosmic Ray Conf. (Pune), 5, 111
———. 2007, in AIP Conf. Proc. 903, Proc. 14th Int. Conf. on Supersymmetry and the Unification of Fundamental Interactions, ed. J. L. Feng (Melville: AIP), 622
Glasstetter, R., et al. 1999, in Proc. 26th Int. Cosmic Ray Conf. (Salt Lake City), 1, 222
Halzen, F., & Zas, E. 1997, ApJ, 488, 669
Hamamatsu Photonics. 1999, Photomultiplier Tubes, Basics and Applications (2nd ed.; Hamamatsu City: Hamamatsu Photonics)
Heck, D. 1999, in Simulation and Analysis Methods for Large Neutrino Telescopes, ed. C. Spiering (Zeuthen: DESY), 228
Henley, E., & Jalilian-Marian, J. 2006, Phys. Rev. D, 73, 094004
Hill, G., & Rawlins, K. 2003, Astropart. Phys., 19, 393
Hörandel, J. 2003, Astropart. Phys., 19, 193
Hundertmark, S. 1999, in Simulation and Analysis Methods for Large Neutrino Telescopes, ed. C. Spiering (Zeuthen: DESY), 276
Kalashev, O., et al. 2002a, Phys. Rev. D, 65, 103003
———. 2002b, Phys. Rev. D, 66, 063004
Kampert, K.-H. 2007, Nucl. Phys. B (Proc. Suppl.), 165, 294
Kashti, T., & Waxman, E. 2005, Phys. Rev. Lett., 95, 181101
Klein, J., & Mann, A. 1999, Astropart. Phys., 10, 321
Klein, S. 2004, preprint (astro-ph/0412546v1)
Kowalski, M., & Gazizov, A. 2005, Comput. Phys. Commun., 172, 203
Kravchenko, I., et al. 2006, Phys. Rev. D, 73, 082002
Kutak, K., & Kwiecinski, J. 2003, European J. Phys. C, 29, 521
Landau, L., & Pomeranchuk, I. 1953, Dokl. Akad. Nauk SSSR, 92, 535
Lipari, P. 1993, Astropart. Phys., 1, 195
Mannheim, K. 1995, Astropart. Phys., 3, 295
Mannheim, K., Protheroe, R. J., & Rachen, J. 2000, Phys. Rev. D, 63, 023003
Migdal, A. 1957, J. Exp. Theor. Phys., 5, 527
Particle Data Group. 2006, J. Phys. G., 33, 1
Pohl, A. C. 2004, Lic. thesis, Kalmar Univ.
Protheroe, R. 1997, in IAU Colloq. 163, Accretion Phenomena and Related Outflows, ed. D. T. Wickramasinghe, G. V. Bicknell, & L. Ferrario (ASP Conf. Ser. 121; San Francisco: ASP), 585 (astro-ph/9607165)
Sigl, G., Lee, S., Bhattacharjee, P., & Yoshida, S. 1998, Phys. Rev. D, 59, 043504
Silvestri, A. 2005, in Proc. 29th Int. Cosmic Ray Conf. (Pune), 5, 431
Stecker, F. 2005, Phys. Rev. D, 72, 107301
Stecker, F., Done, C., Salamon, M., & Sommers, P. 1992, Phys. Rev. Lett., 69, 2738
Tegenfeldt, F., & Conrad, J. 2005, Nucl. Instrum. Methods Phys. Res. A, 539, 407
Wiebel-Sooth, B., Biermann, P., & Meyer, H. 1999, in Interstellar Matter, Galaxy, Universe, ed. W. Martienssen (Berlin: Springer), 37
Yoshida, S., Sigl, G., & Lee, S. 1998, Phys. Rev. Lett., 81, 5505
Zas, E., Halzen, F., & Vázquez, R. 1993, Astropart. Phys., 1, 297